Optical model analyses of 1.65 A GeV argon fragmentation: Cross sections and momentum distributions

L. W. Townsend,[1] F. Khan,[2] and R. K. Tripathi[3]
[1]*NASA Langley Research Center, Hampton, Virginia 23681*
[2]*Old Dominion University, Norfolk, Virginia 23529*
[3]*Christopher Newport University, Newport News, Virginia 23606*
(Received 4 August 1993)

An optical potential fragmentation model capable of predicting fragmentation cross sections and fragment momentum distributions is used to analyze recent measurements of 1.65 A GeV argon projectiles fragmenting in carbon and potassium-chloride targets obtained with the Heavy Ion Spectrometer System (HISS) at the Lawrence Berkeley Laboratory Bevalac. The theoretical model uses an abrasion-ablation-FSI (frictional spectator interaction) collision formalism to estimate elemental and isotopic production cross sections for comparsion with the measured values. The collision momentum transfer model is incorporated into a Goldhaber formalism to analyze measured transverse and longitudinal distributions of the projectile fragments. Good agreement between theory and experiment is obtained for all observables.

PACS number(s): 25.70.Pq, 24.10.Ht

I. INTRODUCTION

The production of fragmentation products in peripheral heavy ion collisions at relativistic energies has been the subject of numerous theoretical and experimental investigations for over two decades. Many of these are summarized in the various reviews that have been written during this period [1–5]. Initial attempts to explain observed fragmentation phenomena invoked statistical models to describe these reactions [6–8]. Later on, these evolved into a two-step model called abrasion-ablation [9], which was based upon earlier work by Serber [10] in the area of inelastic nuclear reactions at high energies. In abrasion-ablation models the abrasion step (particle knockout) is usually formulated using geometric [9,11] or quantum-mechanical arguments [12,13]. In the second stage, the excited prefragment nucleus produced by the abrasion is assumed to decay through particle-emission processes. These are usually modeled using compound nucleus evaporation [9,14] or combined nuclear cascade-evaporation [15] techniques. Alternative approaches based upon nuclear Weiszäcker-Williams methods [16], nucleon-nucleon cascade plus statistical decay models [17], and semiempirical formulations [18–20] have also been proposed.

Over the past several years, we have formulated an optical model description of fragmentation in relativistic heavy ion collisions which can be used to predict both cross sections [13,21] and momentum distributions of the emitted fragments [22,23]. Validation of the model has been hampered by the paucity of available measurements of both cross sections and momentum distributions for the same collision pairs. Heretofore, the most complete set of data was provided by the early measurements for oxygen and carbon beams [24,25] fragmenting in various targets. These data provided values of $d\sigma(0°)/d\Omega$ for isotopes produced by projectile fragmentation in each target and projectile fragment momentum distributions averaged over all of the targets. Comparing model predictions to these measurements for cross sections [26] and momentum widths [22] displayed reasonably good agreement between theory and experiment. Recently, using the Heavy Ion Spectrometer System (HISS) at the Lawrence Berkeley Laboratory Bevalac, high-quality measurements of both cross sections (elemental and isotopic) and fragment momentum distributions for nuclei with mass number $A > 16$ and kinetic energies above 1.0 A GeV have become available [27]. Because of the assumptions underlying abrasion-ablation fragmentation models, these new data should provide a more stringent test of the theory.

In this work the optical potential abrasion-ablation model is described in some detail and used to predict elemental and isotopic fragment production cross sections for comparisons with recently measured values for the breakup of 1.65 A GeV ^{40}Ar projectile ions in carbon (C) and potassium-chloride (KCl) targets [27]. The collision momentum transfers predicted by the model are incorporated into the well-known Goldhaber formalism [7] and the results compared with the measured transverse and longitudinal momentum distributions of the projectile fragments. Excellent agreement between theory and experiment is obtained.

II. FRAGMENTATION CROSS SECTIONS

In an abrasion-ablation collision model, the projectile nuclei, moving at relativistic speeds, collide with stationary target nuclei. At small impact parameters b, portions of their nuclear volumes overlap and are sheared away in the collision. This is the abrasion process. The remaining piece of projectile matter, sometimes called a prefragment, continues its trajectory with essentially its precollision velocity. Because of the nuclear dynamics of the

abrasion process, the projectile prefragment is in an excited state after the collision. This excess energy is removed in the ablation process by the emission of gammas, nucleons, and other particles. The remaining nucleus is the fragment which is experimentally detected.

A. Theory

In the optical potential formalism [13,21] the cross section for producing a prefragment of charge $Z_{\rm PF}$ and mass $A_{\rm PF}$ in the abrasion stage is

$$\sigma_{\rm abr}(Z_{\rm PF},A_{\rm PF})=\binom{N}{n}\binom{Z}{z}\int d^2b[1-T(\mathbf{b})]^{n+z}\times[T(\mathbf{b})]^{A_{\rm PF}}\ , \tag{1}$$

where

$$T(\mathbf{b})=\exp[-A_T\sigma(e)I(\mathbf{b})] \tag{2}$$

and

$$I(\mathbf{b})=[2\pi B(e)]^{-3/2}\int dz_0\int d^3\xi_T\rho_T(\xi_T)\int d^3y\,\rho_p(\mathbf{b}+\mathbf{z}_0+\mathbf{y}+\xi_T)\exp[-y^2/2B(e)]\ . \tag{3}$$

In Eqs. (1)–(3) $\mathbf{b}$ is the impact parameter vector, e is the two-nucleon kinetic energy in their center-of-mass frame, $\mathbf{z}_0$ is the target center-of-mass position in the projectile rest frame, $\xi_i (i=P,T)$ are the internal coordinates of colliding nuclei, A_i $(i=P,T)$ are the mass numbers of colliding nuclei, and $\mathbf{y}$ is the projectile-nucleon-target-nucleon relative separation vector.

The nuclear number densities ρ_i $(i=P,T)$ are extracted from the appropriate charge densities by an unfolding procedure [13] which removes the effects of the finite proton charge distribution. The constituent-averaged nucleon-nucleon cross sections $\sigma(e)$ are also described in Ref. [13]. Values for the diffractive nucleon-nucleon scattering slope parameter $B(e)$ are obtained from the parametrization in Ref. [28].

In Eq. (1) a hypergeometrical charge dispersion model is chosen to describe the distribution of abraded nucleons. The model assumes that z out of Z projectile protons and n out of N projectile neutrons are abraded where

$$N+Z=A_p\ , \tag{4}$$

$$A_{\rm PF}=A_p-n-z\ , \tag{5}$$

and $\binom{A}{B}$ denotes the usual binomial coefficient expression from probability theory. Choosing an alternate charge dispersion model does not alter our results in any significant way.

Prefragment excitation energies are estimated from

$$E_{\rm exc}=E_s+E_{\rm FSI}\ , \tag{6}$$

where the surface energy term (E_s) is calculated using the clean-cut abrasion model of Gosset *et al.* [11]. The frictional-spectator-interaction energy $(E_{\rm FSI})$ contribution is estimated from the model of Oliveira, Donangelo, and Rasmussen [11]. In this model, the rate of energy transfer is given by

$$\frac{dE}{dx}=-\frac{E}{4\lambda}\ , \tag{7}$$

where

$$\lambda=1/\rho\sigma_{NN},\quad \sigma_{NN}\approx 300/E \tag{8}$$

yields

$$\frac{dE}{dx}=-12.75\ \text{MeV/fm}\ . \tag{9}$$

Assuming a spherical nucleus of uniform density, the average energy deposited per FSI is

$$\langle E_{\rm FSI}\rangle=10.2A^{1/3}\ \text{MeV}\ , \tag{10}$$

which yields 35 MeV/FSI for an argon projectile.

Therefore, the abrasion cross section for a prefragment species $(Z_{\rm PF},A_{\rm PF})$ which has undergone p FSI's (where $0\le p\le n+z$) is given by [21]

$$\sigma_{\rm abr}(Z_{\rm PF},A_{\rm PF},p)=\binom{n+z}{p}(1-P_{\rm esc})^p(P_{\rm esc})^{n+z-p}\times\sigma_{\rm abr}(Z_{\rm PF},A_{\rm PF})\ , \tag{11}$$

where $P_{\rm esc}$ is the probability that an abraded nucleon escapes without undergoing any frictional-spectator interactions. In the present work, we choose $P_{\rm esc}=0.5$, which follows from the original work of Oliveira, Donangelo, and Rasmussen [11]. Such a value assumes that there is no curvature of the nuclear surface and should be reasonably correct for heavy nuclei. For lighter nuclei, the surface can exhibit significant curvature such that the value of $P_{\rm esc}$ may be larger than 0.5. Methods for estimating $P_{\rm esc}$ when nuclear surface curvature is taken into account have been formulated by Benesh, Cook, and Vary [29].

Depending upon the magnitude of its excitation energy, the prefragment decays by gamma and/or particle emission channels. The probability $\alpha_{ij}(p)$ that a prefragment species j, which has undergone p FSI's, de-excites to produce a particular final fragment of type i is obtained using the EVA-3 computer code [15]. Therefore, the final hadronic cross section for production of the ith isotopic fragment is obtained from

$$\sigma_{\rm nuc}(Z_i,A_i)=\sum_j\sum_{p=0}^{n+z}\alpha_{ij}(p)\sigma_{\rm abr}(Z_j,A_j,p)\ , \tag{12}$$

where the sum over j accounts for contributions from different prefragments and the sum over p accounts for the effects of $E_{\rm FSI}$. Finally, the elemental production cross sections are obtained by summing over all isotopes

of a given element according to

$$\sigma_{\text{nuc}}(Z_i)=\sum_{A_i}\sigma_{\text{nuc}}(Z_i,A_i)\ . \tag{13}$$

B. Results

Results obtained using Eq. (12) for ^{40}Ar beams at 1.65 A GeV incident kinetic energy fragmenting in carbon and KCl targets are listed in Tables I and II. Also listed are the experimental values [27] obtained using the HISS facility at the Lawrence Berkeley Laboratory Bevalac. The agreement between theory and experiment is quite good, especially considering that there are no arbitrarily adjusted parameters in the theory. Quantitatively, the distributions of isotopic cross-section differences between theory and experiment, for values ≥ 1 mb, are displayed in Table III for both targets. The various entry labels refer to values within the quoted experimental uncertainties, and values outside the quoted uncertainties but within a specified percent difference (e.g., $\leq 25\%$). Overall, over one-third of the predicted cross sections are within the quoted experimental uncertainties, nearly half fall within the error bars or within 25%, and at least 94% agree to within a factor of 2.

Elemental production cross-section predictions obtained using Eq. (13) are compared with experimental values in Figs. 1 and 2. There are two sets of theoretical cross sections displayed. One uses the Rasmussen escape probability ($P_{\text{esc}}=0.5$), which neglects nuclear surface curvature, and the other uses the Vary probability ($P_{\text{esc}}\approx 0.75$), which includes the effects of surface curvature. Overall, the agreement between theory and experiment is nearly the same for either value of P_{esc}, although a quantitative analysis of the distribution of cross section differences, similar to Table III, indicates that the Rasmussen value yields slightly better overall agreement between theory and experiment.

III. FRAGMENT MOMENTUM DISTRIBUTIONS

One of the most significant findings of the early experiments using relativistic oxygen and carbon beams [24,25] was the observation that the fragment momentum distributions were Gaussian in the projectile rest frame. These authors also noted that the experimental momentum distributions were centered at slightly lower momenta values than the incident beams indicating a loss of kinetic energy from the projectile.

TABLE I. Isotope production cross sections in millibarns for 1.65 A GeV argon beams fragmenting in carbon target.

Isotope produced	This work	Experiment Ref. [27]	Isotope produced	This work	Experiment Ref. [27]	Isotope produced	This work	Experiment Ref. [27]
^{39}Cl	65.2	79.5±19.5	^{35}S	26.2	24.0±5.4	^{32}P	31.5	27.0±2.7
^{38}Cl	19.9	8.10±4.05	^{34}S	44.0	49.5±10.8	^{31}P	28.6	21.0±2.1
^{37}Cl	22.0	27.0±8.85	^{33}S	21.9	31.5±7.05	^{30}P	5.5	3.90±0.63
^{36}Cl	64.3	49.5±16.5	^{32}S	2.8	10.6±3.0	^{29}P	0.5	0.315±0.195
^{35}Cl	21.9	51.0±19.5	^{31}S	0.8	0.54±0.42	^{34}Si	0.2	0.01±0.07
^{34}Cl	1.6	12.0±6.45	^{36}P	1.3	0.615±0.195	^{33}Si	1.7	1.32±0.24
^{38}S	7.7	4.35±1.5	^{35}P	1.4	2.10±0.33	^{32}Si	6.6	3.00±0.24
^{37}S	1.8	11.7±2.7	^{34}P	14.6	5.85±0.825	^{31}Si	14.8	11.0±1.8
^{36}S	15.8	12.4±3.0	^{33}P	27.0	18.0±1.8	^{30}Si	24.0	37.5±3.15
^{29}Si	24.8	25.5±3.0	^{26}Al	8.0	7.20±1.28	^{23}Mg	0.9	0.96±0.315
^{28}Si	12.7	13.0±1.95	^{25}Al	0.8	0.315±0.165	^{27}Na	0.2	0.36±0.135
^{27}Si	0.5	0.69±0.285	^{30}Mg	0.1	0.165±0.126	^{26}Na	3.1	2.40±0.51
^{32}Al		0.129±0.111	^{29}Mg	0.3	0.660±0.210	^{25}Na	7.3	7.95±1.05
^{31}Al	1.0	0.705±0.210	^{28}Mg	2.5	2.10±0.495	^{24}Na	14.5	12.6±2.10
^{30}Al	8.0	3.00±0.405	^{27}Mg	6.6	6.75±1.02	^{23}Na	18.5	22.5±3.15
^{29}Al	10.8	10.4±2.25	^{26}Mg	14.5	24.0±2.85	^{22}Na	9.7	8.25±1.65
^{28}Al	20.8	19.5±2.40	^{25}Mg	17.5	22.5±3.45	^{21}Na	0.6	0.255±0.123
^{27}Al	24.3	25.5±2.85	^{24}Mg	10.3	14.2±1.80	^{25}Ne	0.2	0.21±0.146
^{24}Ne	1.0	1.8±0.45	^{21}F	2.3	4.35±0.81	^{18}O	4.3	6.75±1.44
^{23}Ne	5.8	4.8±0.54	^{20}F	10.8	7.20±1.95	^{17}O	12.9	9.75±2.40
^{22}Ne	8.7	12.3±2.25	^{19}F	7.9	11.7±2.25	^{16}O	9.6	14.2±3.45
^{21}Ne	12.4	16.5±2.55	^{18}F	2.9	5.40±1.32	^{15}O	1.0	1.23±0.615
^{20}Ne	5.4	8.55±1.80	^{17}F	1.5	0.345±0.315	^{14}O		0.086±0.111
^{19}Ne	0.4	0.705±0.36	^{20}O		0.330±0.088	^{18}N	0.2	0.60±0.24
^{22}F	0.9	0.765±0.285	^{19}O	2.9	3.60±0.645	^{17}N	1.2	2.25±0.57
^{16}N	7.1	4.65±1.30	^{13}C	12.7	10.0±3.00	^{10}B	2.3	4.05±1.485
^{15}N	17.3	18.0±5.1	^{12}C	7.9	10.2±3.00	^{9}B	0.8	0.495±0.270
^{14}N	14.4	8.7±2.7	^{11}C	0.1	1.215±0.555	^{8}B		0.210±0.255
^{13}N	1.9	0.75±0.48	^{10}C	0.4	0.180±0.240			
^{16}C		0.375±0.165	^{13}B	0.2	1.455±0.555			
^{15}C	0.9	1.17±0.675	^{12}B	2.6	2.25±0.855			
^{14}C	3.5	4.35±1.50	^{11}B	4.7	7.80±2.70			

TABLE II. Isotope production cross sections in millibarns for 1.65 A GeV argon beams fragmenting in KCl targets.

Isotope produced	This work	Experiment Ref. [27]	Isotope produced	This work	Experiment Ref. [27]	Isotope produced	This work	Experiment Re.f [27]
^{39}Cl	82.7	56.0±29.0	^{35}S	30.9	32.0±8.6	^{32}P	38.6	25.0±3.0
^{38}Cl	24.7		^{34}S	60.6	50.0±11.0	^{31}P	30.8	21.0±3.8
^{37}Cl	42.2	42.0±31.0	^{33}S	26.8	41.0±8.5	^{30}P	6.8	7.4±1.7
^{36}Cl	77.1	6.8±3.8	^{32}S	3.9	20.0±6.3	^{29}P	0.8	0.42±0.33
^{35}Cl	25.0	38.0±15.0	^{31}S	0.6	1.9±1.5	^{34}Si	0.3	0.16±0.097
^{34}Cl	1.8	17.0±10.0	^{36}P	1.8	0.2±0.071	^{33}Si	1.8	0.54±0.89
^{38}S	9.5	9.9±2.7	^{35}P	2.3	2.8±0.93	^{32}Si	8.5	1.5±1.8
^{37}S	9.1	19.0±4.1	^{34}P	18.6	2.1±1.5	^{31}Si	20.8	14.0±9.0
^{36}S	18.1	29.0±6.0	^{33}P	35.2	22.0±5.7	^{30}Si	31.2	43.0±5.2
^{29}Si	30.3	38.0±5.2	^{25}Al	0.9	0.86±0.44	^{26}Na	2.7	1.7±1.4
^{28}Si	13.3	15.0±2.8	^{30}Mg	0.2	0.28±0.28	^{25}Na	8.3	5.2±2.9
^{27}Si	1.3	1.4±0.6	^{29}Mg	0.3	0.68±0.34	^{24}Na	20.0	19.0±4.3
^{31}Al	1.1	0.58±0.32	^{28}Mg	2.8	0.42±0.8	^{23}Na	23.1	30.0±5.9
^{30}Al	7.8	1.5±0.49	^{27}Mg	10.6	10.0±4.7	^{22}Na	12.2	12.0±2.2
^{29}Al	14.6	22.0±5.3	^{26}Mg	18.6	29.0±3.2	^{21}Na	0.7	0.76±0.8
^{28}Al	26.0	18.0±4.7	^{25}Mg	22.1	26.0±3.9	^{25}Ne		0.40±0.37
^{27}Al	28.1	37.0±4.3	^{24}Mg	12.4	21.0±3.5	^{24}Ne	1.4	1.4±0.51
^{26}Al	10.3	8.0±1.3	^{23}Mg	1.2	0.4±0.18	^{23}Ne	5.6	5.5±1.7
^{22}Ne	10.0	16.0±2.7	^{20}O	0.8	0.99±0.30	^{14}N	16.5	12.0±5.3
^{21}Ne	16.5	25.0±4.5	^{19}O	3.0	6.1±1.4	^{13}N	1.6	1.2±0.76
^{20}Ne	6.4	14.0±3.3	^{18}O	5.7	8.3±2.5	^{16}C		0.02±0.48
^{19}Ne	0.5	0.46±0.24	^{17}O	14.4	17.0±3.8	^{15}C	1.1	2.8±0.98
^{22}F	0.9	2.2±0.93	^{16}O	9.7	24.0±6.1	^{14}C	3.6	4.0+2.7
^{21}F	2.9	4.6±1.7	^{15}O	1.4	2.0±1.1	^{13}C	13.2	13.0±4.2
^{20}F	11.7	9.1±1.9	^{17}N	1.5	4.8±0.73	^{12}C	6.2	14.0±6.0
^{19}F	9.6	16.0±3.3	^{16}N	7.7	7.7±3.1	^{11}C	0.7	1.50±0.67
^{18}F	3.1	5.8±2.0	^{15}N	20.9	27.0±7.0	^{10}C	0.1	0.48±0.55
^{13}B		1.9±2.0						
^{12}B	1.9	1.6±1.7						
^{11}B	2.8	11.0±3.7						
^{10}B	2.2	5.6±1.8						
^{9}B	0.5	1.2±0.88						

Initial attempts to explain the observed momentum distributions included statistical fragmentation models [6,7] and a model based upon the sudden approximation of quantum mechanics [30]. Assuming only that momentum conservation holds and that the original fragmenting nucleus was a Fermi gas of uncorrelated nucleons, Goldhaber [7] demonstrated that the observed momentum distributions of the fragments were independent of the speed of the fragmentation process. Furthermore, it was

TABLE III. Distribution of isotopic cross section differences between theory and experiment for 1.65 A GeV argon beams fragmenting in carbon and KCl targets.

Percent Difference	Percentage of cross sections Carbon target	KCl target
Within error bars	34	45
≤25[a]	9	4
26–50[a]	36	22
51–100[a]	15	23
>100[a]	6	6

[a]Outside error bars but within specific percent difference band.

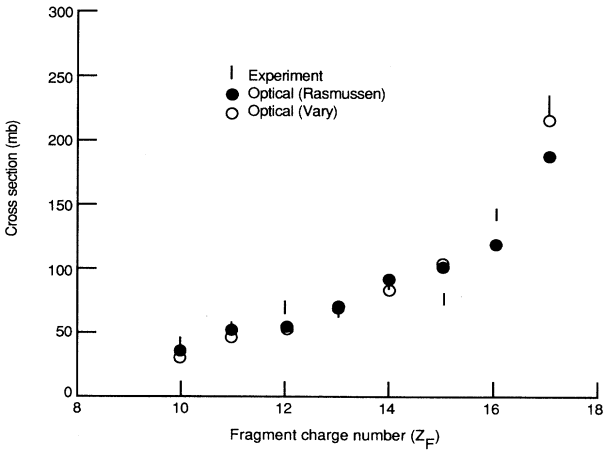

FIG. 1. Elemental production cross sections for argon projectiles fragmenting in carbon targets. The optical model predictions use the Oliveira-Donangelo-Rasmussen [11] and Benesh-Cook-Vary [29] escape probability prescriptions.

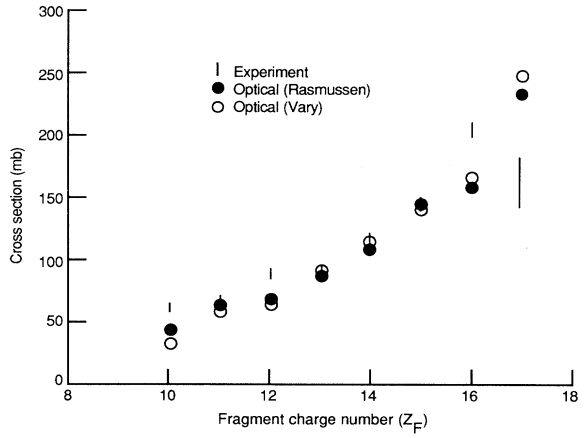

FIG. 2. Elemental production cross sections for argon projectiles fragmenting in KCl targets. The optical model predictions use the Oliveira-Donangelo-Rasmussen [11] and Benesh-Cook-Vary [29] escape probability prescriptions.

found that the theory [7] predicted that the momentum distributions of the heavy fragments were most sensitive to the collision momentum transfers. Thus, the width h_j of the Gaussian momentum distribution in any direction would be modified by a mean squared momentum transfer Q_j^2 in that direction according to

$$(h_j')^2 = h_j^2 + \frac{A_F^2 Q_j^2}{A_p^2} , \tag{14}$$

where A_F is the fragment mass number and A_p is the mass of the fragmenting nucleus (note that we use the symbol h, instead of σ, to avoid confusion with the cross-section expressions in the previous sections of this paper). Similarly, the mean of the distribution is modified as

$$P_j' = P_j + \left[\frac{A_F}{A_P}\right] Q_j . \tag{15}$$

From the latter, the longitudinal down shift (loss) is given by

$$P_{\text{loss}} = \frac{A_F}{A_P} Q_{\parallel} , \tag{16}$$

where $Q_{\parallel}$ is the magnitude of the longitudinal momentum transfer.

Subsequent modifications of Goldhaber's theory incorporated Pauli correlation effects [31] and phase-space constraints [32] in the final states. Both modifications narrow the predicted momentum widths from the Goldhaber values.

Until recently, reported measurements of momentum distributions were limited to longitudinal distributions [25,33]. Although both experiments noted that the transverse widths were approximately equal to the longitudinal widths (within $\approx 10\%$), neither experiment measured the transverse momentum distributions accurately enough to draw definitive quantitative conclusions.

Several years ago, measurements of transverse momentum distribution widths for fragments produced in the breakup of 1.2A GeV ^{139}La projectiles were reported [34]. In that experiment, it was observed that the momentum distributions were much wider than those predicted by either the Goldhaber [7] or Lepore-Riddell [30] models. Recent measurements of longitudinal and transverse momentum distributions for fragments produced in the breakup of 1.65A GeV ^{40}Ar projectiles in carbon and KCl targets have also been reported [27]. The longitudinal momentum downshifts were found to be consistent with the momentum downshifts observed by Greiner *et al.* [25]. The measured widths of the longitudinal and transverse momentum distributions were consistent in magnitude with Goldhaber's theory but larger than those predicted by the theory of Lepore and Riddell, and also larger than those predicted using Murphy's phase-space constraint argument. More recently, data on transverse momentum distribution widths for Au+C, Au+Mg, and Nb+C collisions at relativistic energies also indicate that Goldhaber theory based upon internal Fermi momentum alone cannot explain the observations [35].

A. Theory

In previous work [22,23], we used the impulsive excitation energy ideas of Fricke [36], within the context of composite particle multiple-scattering theory, to derive an optical potential method of predicting momentum transfers in relativistic heavy ion collisions. Using this method as input into the Goldhaber formalism, fragment momentum downshifts and widths were estimated [22] and compared with the reported measurements for oxygen and carbon beams [25] on various targets and for lanthanum beams on carbon targets [34]. Very good agreement between theory and experiment was obtained. In the present work, the model is used to estimate longitudinal momentum downshifts and momentum distribution widths which are compared with measured downshifts and widths for Ar+C and Ar+KCl collisions.

From Eq. (19) of Ref. [22], the magnitudes of the longitudinal momentum loss (transfer) is

$$P_{\text{loss}} = (Q_{\text{Im}} - Q_R)^{1/2} , \tag{17}$$

where

$$Q_{\text{Im}}(e,b) = -A_P A_T \int d^3\xi_P \rho_P(\xi_P) \int d^3\xi_T \rho_T(\xi_T) \nabla_P \int_{-\infty}^{\infty} \text{Im}\tilde{t}(\mathbf{b}+\mathbf{z}'+\xi_P-\xi_T)\frac{dz'}{v} \tag{18}$$

and

$$Q_R(e,b) = -A_P A_T \int d^3\xi_P \rho_P(\xi_P) \int d^3\xi_T \rho_T(\xi_T) \nabla_P \int_{-\infty}^{\infty} \text{Re}\tilde{t}(e,\mathbf{b}+\mathbf{z}'+\xi_P-\xi_T)\frac{dz'}{v} . \tag{19}$$

In Eqs. (18) and (19) the nuclear densities ρ_i ($i=P,T$) are normalized to unity, the A_i are the mass numbers of the colliding nuclei, and v is their relative velocity. The gradient is taken with respect to the projectile internal coordinates ξ_P, and $\tilde{t}$ is the complex constituent-averaged two-nucleon transition amplitude. The latter is parametrized in the usual way as

$$\tilde{t}(e,\mathbf{x})=-(e/m)^{1/2}\sigma(e)[\alpha(e)+i][2\pi B(e)]^{-3/2} \times\exp[-x^2/2B(e)] , \quad (20)$$

where $\sigma(e)$ and $B(e)$ were described after Eq. (13) and $\alpha(e)$ is the ratio of the real-to-imaginary part of the forward scattering amplitude. At an energy of 1.65 A GeV $\alpha(e)\approx 0.32$.

At energies $\leq 400A$ MeV, nonlocal effects and the concomitant modifications of the nucleon-nucleon interaction are important. Also, compression effects lead to higher densities of the system. To account for these effects, and to account for the disappearance of collective flow effects at certain energies called balance energies, we defined the total transverse momentum transfer as [37]

$$Q_\perp(e,b)=Q_R(e,b)-Q_R(E_0,b) , \quad (21)$$

where E_0, the balance energy for the system, is estimated from systematics [37].

B. Results

In this work, momentum transfer components given by Eqs. (17) and (21) are used in Eqs. (14) and (16) to predict momentum distribution widths and longitudinal downshifts. Following the methods of Ref. [22], the most probable impact parameters for each fragmentation channel, used as inputs into the momentum transfer expressions, are obtained from a semiempirical, abrasion-ablation fragmentation model (NUCFRAG) [20]. For consistency, the uniform, spherical density distributions used in NUCFRAG are also used to solve Eqs. (18) and (19).

Analyses of momentum distribution variances or "widths" are typically presented in terms of a reduced width h_0 related to the total width h' [from Eq. (14)] according to

$$(h')^2=h_0^2 A_F(A_P-A_F)/(A_P-1) . \quad (22)$$

Figures 3 and 4 display experimental reduced widths for momenta transverse (x,y) to the beam (z) direction [27] versus fragment mass number. Also displayed are theoretical values obtained by assuming that

$$Q_x=Q_y=Q_\perp/\sqrt{2} , \quad (23)$$

which is consistent with the experimental findings [27]. The procedure used to obtain these theoretical estimates is to compute $Q_\perp$ using Eqs. (19) and (21). Equation (23) is then used to estimate Q_x and Q_y, which are, in turn, inserted into the right-hand side of Eq. (14). Another input into the right side of Eq. (14) is the intrinsic width h_j ($j=x,y$). These are usually estimated using statistical [7] or sudden approximation [30] models. In this work we use a modified Lepore-Riddell model [30] where the oscillator spacing is obtained from experimentally measured nuclear radii. For argon projectiles, the intrinsic width term is given by [38]

$$h_j=70.7[A_F(A_P-A_F)/(A_P-1)]^{1/2} , \quad (24)$$

where $A_P=40$. The agreement between theory and experiment displayed in Figs. 3 and 4 is very good.

Unlike transverse momentum distributions which are Lorentz invariant and have zero means in the projectile rest frame, longitudinal distributions are not Lorentz invariant and have means which are downshifted with respect to the projectile rest frame. Results for argon fragmentation longitudinal momentum downshifts, in the

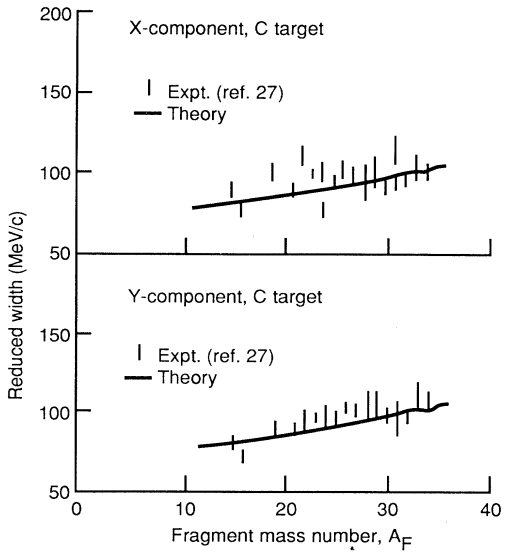

FIG. 3. Reduced transverse momentum widths as a function of fragment mass number for the carbon target.

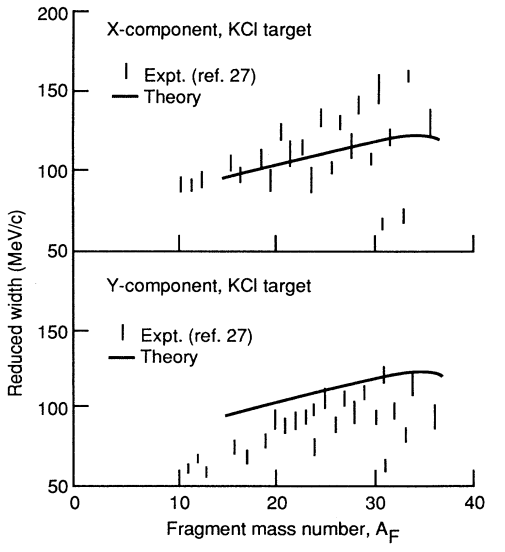

FIG. 4. Reduced transverse momentum widths as a function of fragment mass number for the KCl target.

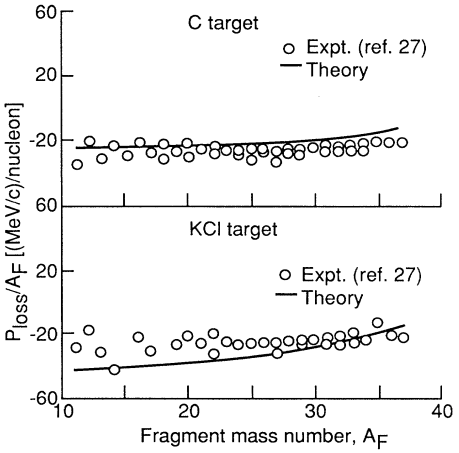

FIG. 5. Fragment longitudinal momentum downshifts per nucleon as a function of fragment mass number.

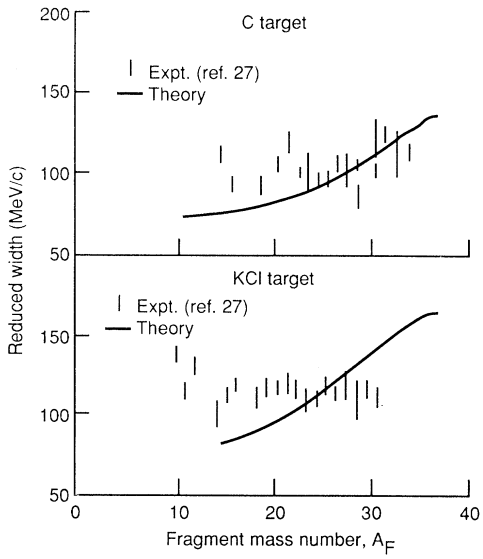

FIG. 6. Reduced longitudinal momentum widths as a function of fragment mass number.

rest frame, are displayed in Fig. 5 as a function of fragment mass number. Also displayed are the experimental values obtained with the HISS detector [27]. The agreement between theory and experiment is good, considering the simplified form of the nuclear densities used for the calculations, and considering the absence of adjustable parameters in the theory. The calculated means of the downshifts are -15 MeV/c nucleon for the carbon target and -22 MeV/c nucleon for the KCl target. These are in good agreement with the experimental values of -26.1 ± 3.7 MeV/c nucleon (carbon target) and -24.2 ± 5.1 MeV/c nucleon (KCl target). The use of simple uniform densities, which poorly represent the carbon nucleus, probably accounts for most of the disagreement between the values for the carbon target.

To calculate the longitudinal momentum widths of the fragments, the mean squared momentum transfer in the longitudinal direction is needed [7]. From physics considerations, this is the energy-momentum transfer associated with the width of the prefragment excitation. From Eq. (18) of Ref. [22], this is

$$Q_z^2=2Q_R Q_{\rm Im} \ . \tag{25}$$

Incorporating Eq. (25) into Eq. (14) and using Eq. (22) to extract h_0 yields the estimate displayed in Fig. 6. Also shown are the experimental values [27]. The agreement between theory and experiment is very good for the carbon target and only fair for the KCl target. All displayed values are given in the projectile rest frame.

Overall, the agreement between theory and experiment for these momentum observables is very good; however, some differences do exist. There is good agreement for the carbon target longitudinal widths but only fair agreement for the downshifts. For the KCl target the converse is true. There we note excellent agreement for the downshifts but only fair agreement for the widths. Finally, for the transverse width components, there is very good agreement between theory and experiment for both targets. Clearly, additional experimental data for other nucleus-nucleus collision pairs would be useful for understanding and resolving the differences.

IV. CONCLUDING REMARKS

Comparing theory with measurements for both fragmentation cross sections and momentum distributions provides a more stringent test than comparisons with either alone. For the first time, optical potential fragmentation model predictions for both categories of observables have been directly compared with precise data for both types of observables obtained in a single heavy ion fragmentation experiment. Overall, the agreement between theory and experiment was excellent considering the total lack of arbitrary fitting parameters in the model. These results suggest that optical potential, abrasion-ablation models can be reliably used to describe heavy ion fragmentation reaction observables. The availability of additional experimental data of the quality of these argon measurements is eagerly awaited.

ACKNOWLEDGMENTS

Useful discussions with C. E. Tull about the experimental data are gratefully acknowledged.

[1] A. S. Goldhaber and H. H. Heckman, Annu. Rev. Nucl. Part. Sci. **28**, 161 (1978).
[2] S. Nagamiya, J. Randrup, and T. J. M. Symons, Annu. Rev. Nucl. Part. Sci. **34**, 155 (1984).
[3] J. Hüfner, Phys. Rep. **125**, 129 (1985).
[4] G. Baür, F. Rosel, D. Trautmann, and R. Shyam, Phys. Rep. **111**, 333 (1984).
[5] *Treatise on Heavy-Ion Science,* edited by D. Allan Bromley (Plenum, New York, 1984–1989), Vols. 1–8.
[6] H. Feshbach and K. Huang, Phys. Lett. **47B**, 300 (1973).
[7] A. S. Goldhaber, Phys. Lett. **53B**, 306 (1974).
[8] R. K. Bhaduri, Phys. Lett. **50B**, 211 (1974).

[9] J. D. Bowman, W. J. Swiatecki, and C. F. Tsang, Lawrence Berkeley Laboratory Report No. LBL-2908, 1973 (unpublished).
[10] R. Serber, Phys. Rev. **72**, 1114 (1947).
[11] J. Gosset, H. H. Gutbrod, W. G. Meyer, A. M. Poskanzer, A. Sandoval, R. Stock, and G. D. Westfall, Phys. Rev. C **16**, 629 (1977); L. F. Oliveira, R. Donangelo, and J. O. Rasmussen, *ibid.* **19**, 826 (1979).
[12] J. Hüfner, K. Schäfer, and B. Schürmann, Phys. Rev. C **12**, 1888 (1975); M. Bleszynski and C. Sander, Nucl. Phys. **A326**, 525 (1979).
[13] L. W. Townsend, Can. J. Phys. **61**, 93 (1983); L. W. Townsend, J. W. Wilson, and J. W. Norbury, *ibid.* **63**, 135 (1985).
[14] J.-J. Gaimard and K.-H. Schmidt, Nucl. Phys. **A531**, 709 (1991).
[15] D. J. Morrissey, L. F. Oliveira, J. O. Rasmussen, G. T. Seaborg, Y. Yariv, and Z. Fraenkel, Phys. Rev. Lett. **43**, 1139 (1979).
[16] H. Feshbach and M. Zabek, Ann. Phys. **107**, 110 (1977).
[17] B. G. Harvey, Phys. Rev. C **45**, 1748 (1992).
[18] R. Silberberg, C. H. Tsao, and M. M. Shapiro, in *Spallation Nuclear Reactions and Their Applications,* edited by B. S. P. Shen and M. Merker (Reidel, Dordrecht-Holland, 1976), pp. 49–81.
[19] J. R. Cummings, W. R. Binns, T. L. Garrard, M. H. Israel, J. Klarmann, E. C. Stone, and C. J. Waddington, Phys. Rev. C **42**, 2530 (1990).
[20] J. W. Wilson, L. W. Townsend, and F. F. Badavi, Nucl. Instrum. Methods B **18**, 225 (1987).
[21] L. W. Townsend, J. W. Wilson, F. A. Cucinotta, and J. W. Norbury, Phys. Rev. C **34**, 1491 (1986); L. W. Townsend, J. W. Norbury, and F. Khan, *ibid.* **43**, R2045 (1991); J. W. Norbury and L. W. Townsend, *ibid.* **42**, 1775 (1990).
[22] F. Khan, G. S. Khandelwal, L. W. Townsend, J. W. Wilson, and J. W. Norbury, Phys. Rev. C **43**, 1372 (1991).
[23] L. W. Townsend, J. W. Wilson, F. Khan, and G. S. Khandelwal, Phys. Rev. C **44**, 540 (1991).
[24] P. J. Lindstrom, D. E. Greiner, H. H. Heckman, Bruce Cork, and F. S. Beiser, Lawrence Berkeley Laboratory Report No. LBL-3650 (1975) (unpublished).
[25] D. E. Greiner, P. J. Lindstrom, H. H. Heckman, Bruce Cork, and F. S. Beiser, Phys. Rev. Lett. **35**, 152 (1975).
[26] L. Townsend, J. W. Wilson, F. A. Cucinotta, and J. W. Norbury, NASA Technical Memorandum No. TM-87692, 1986 (unpublished).
[27] C. E. Tull, "Relativistic Heavy Ion Fragmentation at HISS," Ph.D. thesis, Lawrence Berkeley Laboratory Report No. LBL-29718, 1990 (unpublished).
[28] F. E. Ringia, T. Dobrowolski, H. R. Gustafson, L. W. Jones, M. J. Longo, E. F. Parker, and Bruce Cork, Phys. Rev. Lett. **28**, 185 (1972).
[29] C. J. Benesh, B. C. Cook, and J. P. Vary, Phys. Rev. C **40**, 1198 (1989).
[30] J. V. Lepore and R. J. Riddell, Jr., Lawrence Berkeley Laboratory Report No. LBL-3086, 1974 (unpublished).
[31] G. Bertsch, Phys. Rev. Lett. **46**, 472 (1981).
[32] M. J. Murphy, Phys. Lett. **135B**, 25 (1984).
[33] Y. P. Viyogi *et al.*, Phys. Rev. Lett. **42**, 33 (1979).
[34] F. P. Brady *et al.*, Phys. Rev. Lett. **60**, 1699 (1988).
[35] F. P. Brady *et al.*, Bull. Am. Phys. Soc. **37**, 1266 (1992).
[36] S. H. Fricke, Ph.D. dissertation, University of Minnesota, 1985 (unpublished); B. F. Bayman, P. J. Ellis, S. Fricke, and Y. C. Tang, Phys. Rev. Lett. **53**, 1322 (1984).
[37] R. K. Tripathi, L. W. Townsend, and F. Khan, Phys. Rev. C **47**, R935 (1993); F. Khan, L. W. Townsend, R. K. Tripathi, and F. A. Cucinotta, *ibid.* **48**, 926 (1993).
[38] R. K. Tripathi, L. W. Townsend, and F. Khan (unpublished).